Materials Research. 2021; 24(5):e20210034
DOI: https://doi.org/10.1590/1980-5373-MR-2021-0034

Mechanical Preparation Procedure for Characterizing by EBSD the Crystallographic Orientation in Surface Layers of Austenitic Stainless Steels Plasma Nitrided

Rafael R. Fischer[a], Abel A. C. Recco[a,]*, Carlos M. Garzón[b]

[a]*Universidade do Estado de Santa Catarina UDESC, Departamento de Física, Joinville, SC, Brasil.*
[b]*Universidad Nacional de Colombia UNal, Departamento de Física, Bogotá D.C., Colombia.*

Received: January 12, 2021; Revised: July 14, 2021; Accepted: August 04, 2021

This contribution reports on an experimental polishing procedure, that is comprised of early grinding in Al_2O_3 slurries and late polishing in colloidal silica, which is used for preparing the nitrided region of a plasma nitrided austenitic stainless steel, for crystallographic analysis via electron backscatter diffraction (EBSD). The suitability of the polished surfaces for conducting EBSD characterization was assessed through an analysis of both the surface roughness (appraised by atomic force microscopy) and the quality of the Kikuchi diffraction patterns. We observed that as-nitrided virgin surfaces were not suitable for EBSD characterization, due to intense surface roughening, which was induced by the nitriding process itself. At the subsurface region, exposed by on-top mechanical polishing, the flatter nature of the polished surfaces allowed the acquisition of EBSD patterns with enough quality for microtexture analysis. A resolution of 100 nm in the total removed layer was attainable via careful control of the polishing parameters. Close parallelism between the polished and original surfaces was verified.

Keywords*: Electron backscatter diffraction, orientation imaging microscopy, metallography, scanning electron microscopy, mechanical polishing.*

1. Introduction

Electron backscatter diffraction (EBSD) enables an assessment of the crystallographic orientation of microstructure in diverse alloys[1-3]. EBSD characterization is performed in a scanning electron microscope (SEM), which is equipped with a system that is capable of registering and indexing Kikuchi diffraction patterns. Nowadays, the effect of diverse thermomechanical and thermochemical processes on the crystallographic character of the microstructure is routinely assessed by EBSD[4-7].

Sample preparation is a limiting step in EBSD characterization[8-10]. Samples should be flat in a nanometer length, and substructures should have a moderate concentration of defects[11,12]. This hinders the EBSD characterization of diverse metallurgical structures. Material surfaces altered by work-hardening exhibit impaired Kikuchi diffraction patterns[13,14]. Surface topography can either decrease the quantity of electrons reaching the phosphorous screen[15] or induce gradients of intensity in the interior of actual EBSD patterns[16]. Thus, samples with roughened surface topography could present not indexable EBSD patterns[15,16].

EBSD is granted as a mature standard technique for orientation microscopy and texture characterization in polycrystalline materials[3]. Phase identification can be also carried out in crystalline materials, mainly when associated to a simultaneous elemental mapping[2]. However, EBSD lacks accuracy for carrying out unambiguous phase characterization in diverse materials. EBSD is less accurate as compared to XRD[3]. EBSD provides not as rich crystallographic information as it is provided by electron diffraction in the transmission electron microscope[4,9]. Many dispersed phases could not be characterized by EBSD because they do not provide clear enough EBSD patterns[4,9]. Because of that, Stojakovic claims for differentiating between (a) phase verification and (b) phase identification[2]. "In phase verification there is a great deal of certainty of phases presents in material, therefore only several (preselected) choices are searched in crystallographic database. On the other hand in phase identification there is a great deal of uncertainty of phases present and a large database of crystalline compounds would need to be searched for a good match, which would be impractical"[2]. In particular, in austenitic steel structures containing colossal dissolution of nitrogen, EBSD technique is not accurate enough to characterize the lattice expansion neither the lattice distortion reported with XRD analysis as a basis[17-19]. Austenitic steel structures containing colossal dissolution of nitrogen could contain dispersion of nanometric nitrogen-rich compound phases[17]. A complete unambiguous characterization of the nitrogen-rich austenitic steel structure demands for the using of diverse complementary characterization techniques, like XRD or TEM, being not possible to fully identify the phases present by EBSD characterization[17-19].

In this contribution, we report on the suitability of the EBSD technique for crystallographic characterization of the grain orientation in the nitrided region of an austenitic stainless steel (ASS). The main factors making difficult the EBSD characterization of nitrided cases in ASSs are the indigenous rough nature of the as-nitrided surfaces and the

*e-mail: abel.recco@udesc.br

nitriding-induced plastic deformation of the microstructure at the surface regions.

Plasma nitriding of ASSs is a thermochemical process that aims at improving anti-scratch and anti-wear properties of conventional ASSs. When carried out at temperatures lower than around 400 °C (673 K), plasma nitriding of ASSs allows one to obtain materials with an overall high toughness, and high hardness at the surface region, without meaningful deterioration of the corrosion resistance[17,20-22].

Plasma nitriding induces modifications of the crystallographic structure of ASSs. This has been observed by conventional X-ray diffraction (XRD)[23,24] and EBSD[18,25]. Stinville et al.[18] reported rotation of grains in ASSs because of plasma nitriding, which was induced by the colossal dissolution of nitrogen. They prepared the nitrided case of an ASS for both EBSD and nanohardness analyses through mechanical polishing, grinding a 5-µm-thick layer from the virgin surface[25].

EBSD characterization through serial sectioning is a well-documented technique[26-28]. This consists of the early removal of superficial layers with a homogeneous thickness and the later analysis of crystallographic structures of the new surfaces. The removal of layers with a well-defined thickness and the retrieval of new surfaces with controlled parallelism, with regard to the virgin surface, are prerequisites for appropriate serial sectioning characterization. Serial sectioning is commonly carried out through electrochemical polishing[29], focused ion beam[30], and mechanical polishing[25].

In this contribution, we report on sample preparation, through mechanical polishing, for crystallographic characterization of the microstructure of ASS samples nitrided at 400 °C. The surface roughness and EBSD pattern quality of polished surfaces are assessed. Both annealed (for comparison) and plasma nitrided samples are studied. The aim of the research is to appraise the suitability of mechanical polishing for preparing the nitrided surfaces for characterizing the crystallographic orientation of the austenitic grains, through EBSD experiments. We report on an optimized polishing method that is used for obtaining well-defined Kikuchi diffraction patterns, after removing layers 1.4 µm thick. Although the already published mechanical serial sectioning practices can be adapted for preparing the nitrided case for EBSD analysis[18,25,26], the processes reported in this contribution outperforms that previous ones in high resolution of the removed layer, thinner removed layers after nitriding and (the most important improvement) negligible deviation from the parallelism between the grinded and the as-nitrided virgin surfaces.

2. Experimental

2.1. Plasma nitriding

Table 1 depicts the chemical composition of the steel studied, namely ASS UNS S30400.

The starting material was an annealed bar that was 35 mm in diameter. Samples of 10-mm width were cut from the initial bar, and then they were mechanically polished. Samples were cut using a Isomet 1000 precision cutter facility, which allows sample refrigeration.

The metallographic preparation consisted of emery paper grinding, followed by diamond paste polishing, with a final polishing stage in a slurry containing Al_2O_3, with a 1-µm average particle diameter. After that, the samples were subsequently washed in water and isopropyl alcohol. Then, they were cleaned in an ultrasonic bath filled with acetone, cleaned again in water and isopropyl alcohol, and finally, dried under hot air.

The cleaned samples were charged into a stainless steel vacuum chamber, and then, the chamber was closed and evacuated up to 100 Pa by using a mechanical pump with pumping capacity of 18 $m^3 \cdot h^{-1}$. After the base pressure was attained, the samples were heated at 613 K. Then a sputtering stage was carried out for 1 h with the aim of cleaning the sample surface from oxides and absorbed impurities. At that cleaning stage a gas flux of 75%-vol of H_2 + 25%-vol of Ar was stablished, which increased chamber pressure to 400 Pa. Subsequently, sample temperature was increased up to 673 K and the samples were plasma nitrided by using a H_2 + N_2 gas mixture, which contained 25%-vol of N_2 at a chamber pressure of 400 Pa. Nitriding time was set at 1.5 h. A direct current power source was used. Voltage and current were around 400 V and 4.5 mA, respectively. After nitriding, the samples were cooled inside the vacuum chamber with no flux of gases. Temperature decreased from 673 to 300 K in around 2 h.

2.2. Fiduciary indentation marks for assisting the polishing process

Fiduciary indentation marks were indented on top of each analyzed sample, with the aim of (i) assisting the positioning during both AFM and SEM-EBSD experiments and (ii) appraising the depth of the layer ground. Indentations with two different sizes were carried out. Bigger Vickers indentations (carried out with 5.1 N load) were imprinted on the samples resembling a coordinate system. Smaller Berkovich indentations (carried out with 0.04 N load) were imprinted on the samples as reference marks for assessing the depth of the layer ground. Figure 1 shows the surface appearance, observed in the SEM facility, of one of the samples studied, where five Vickers indentations and nine Berkovich indentations can be observed. Via AFM, the difference of residual indentation depth between the final and initial surface for each polishing stage was assessed, and that was assumed as the thickness removed. The reader is advised that Vickers indentations were used as a reference frame, and they were not used for assessing the depth of the removed layer due to polishing.

Table 1. Chemical composition of the steel studied, UNS S30400 austenitic stainless steel, wt-%.

P	S	C	Si	Mn	Ni	Cr	Fe
< 0.005	< 0.022	0.06	0.4	1.1	8.1	18.1	Bal.

***** Error in individual specie content is around 5 to 10% of nominal content.

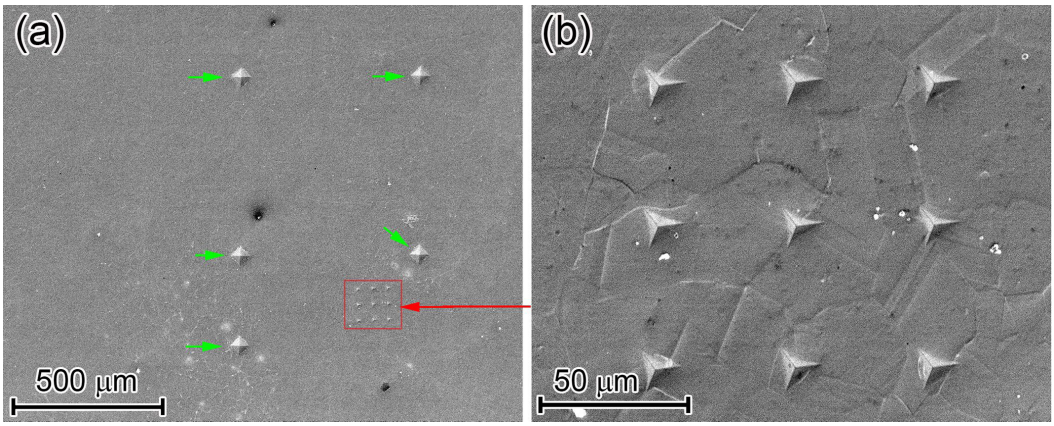

Figure 1. Scanning electron micrographs of the region with fiduciary indentation marks. Five Vickers imprints (green arrows, left inset) and nine Berkovich imprints (red arrow, left, and the concomitant enlarged inset, right) can be seen. Not chemical etching. Secondary electrons. 15 kV. 25 mm working distance.

2.3. Grinding and polishing

Nitrided samples as well as annealed samples (for comparison) were ground into a slurry containing Al_2O_3 abrasive with an average particle size of 1 µm.

Preliminary grinding tests, varying the grinding time (0.5, 0.75, and 2 h) and the concentration of Al_2O_3 in the slurry, were carried out. Then, a specific grinding condition was selected, on the basis of the SEM- and AFM-assessed surface appearance and wear rate. Definitive results presented in this contribution were obtained with a grinding time of 0.75 h and a slurry containing 10 ml of Al_2O_3 suspension and 300 ml of distilled water. Shorter grinding times gave very rough surfaces, whereas longer grinding times lead to very thick removed layers. Grinding slurries with a higher concentration of Al_2O_3 resulted in increased wear rates but displayed structures that were very rough at the grain size length.

The ground samples were washed in water with a neutral washing-up liquid. The samples were then polished into an abrasive slurry containing colloidal silica, with an average particle size of 0.05 µm. Polishing time was either 17 h or 34 h. The polishing slurry was prepared by mixing 10 ml of colloidal silica suspension with 300 ml of distilled water. Special care was taken for using a non-agglomerated colloidal silica suspension. The polishing stage was finished by washing the samples in water with a neutral washing-up liquid, ultrasonically cleaning in isopropyl alcohol, cleaning again in water with a neutral washing-up liquid, and drying under hot air. Special care was taken during the period of washing the samples with washing-up liquid for obtaining silica-free surfaces.

Both the grinding and polishing stages were carried out by using a commercially available vibratory polishing facility, Vibromet®, provided by Buehler. The vibratory intensity was set at 60% (a.u), and the weight of the sample holder was set at 0.41 kg. Thus, the nominal pressure during grinding and polishing was around 40.2 kPa. A homogenous distribution of the holder weight over the sample was verified.

No pitting corrosion was observed in the polished surfaces. The polishing cloth and the polishing machine were cleaned with abundant water.

2.4. Atomic force microscopy

An atomic force facility NanoSurface, NANITE-B, was used for both (i) appraising the surface roughness at the different stages of the sample preparation and (ii) profiling the inside of the Berkovich indentations.

AFM micrographs were obtained by scanning a 70 µm x 70 µm area with 256 scanned points per line, at 1 scanned line per second. Both x-axis and y-axis scans were identical. Scans were carried out with the non-contact mode. The AFM facility used had a typical resolution of around 0.1 nm in the vertical direction (z-axis).

2.5. Electron backscattering diffraction

The crystallographic orientation of microstructures in square regions that were 0.6 x 0.6 mm^2 was assessed by EBSD. An Oxford EBSD system, NordlysNano, implemented in a field emission gun scanning electron microscope (FEG-SEM), was used. A Jeol JSM-6701F FEG-SEM was used. Sample surfaces were tilted 70° with regard to a horizontal reference line.

A squared scanning grid, with 3 µm of scanning step, was used. The following FEG-SEM operational parameters were used: 25 kV acceleration voltage, 20 µA probe current, and 15 mm working distance.

Each Kikuchi diffraction pattern analyzed was the average of four live patterns. Ten diffraction bands were indexed for each diffraction pattern. The scanning speed obtained was around 21 indexed patterns by s.

At some representative points in the microstructure, the appearance of individual Kikuchi diffraction patterns and the Hough transform of them were assessed.

The recorded EBSD data were post-processed via the Channel five suit of programs, provided by HKL. The following microstructure features were appraised: (i) grain boundary character and morphology, (ii) microtexture, (iii) spatial orientation of individual grains, and (iv) the local misorientation. The user manual of the Channel five suit of programs provides enough information for reproducing the aforementioned EBSD analysis.

The samples were assumed to be formed by the FCC γ steel phase, with symmetry Fm-3m (225 space group).

2.6. X-ray diffraction

Crystallographic structure characterization was performed through X-ray diffraction experiments, using a Philips PW 1710 conventional diffractometer. X-ray experiments, in the Bragg–Brentano configuration, were carried out with monochromatic radiation Cu K-α, λ= 1.54056 Å, generator voltage of 40 kV, and generator current of 30 mA. XRD scans were carried out at a 0.02° angular step, 2 s swept time for each angular position, and scanning Bragg angles, 2θ, varying between 20° and 90°.

3. Results

3.1. Thickness, mechanical properties and structure of the nitrided case

Figure 2 shows an SEM micrograph of the transverse section of a sample nitrided. The thickness of the nitrided layer was 9.5±1.5 µm. Via AFM, the difference of residual indentation depth between the final and initial surface for each polishing stage was assessed, and that was assumed as the thickness removed. It was observed that the thickness removed (lower than 1.5 µm) is around 15% of the thickness of the nitrided case (9.5 µm). The interaction volume, i.e. the region where the signal affecting the EBSD patterns is generated, has been depicted as a cylinder around 10-50 nm depth, with surface area similar to that of the incident beam[2,4].

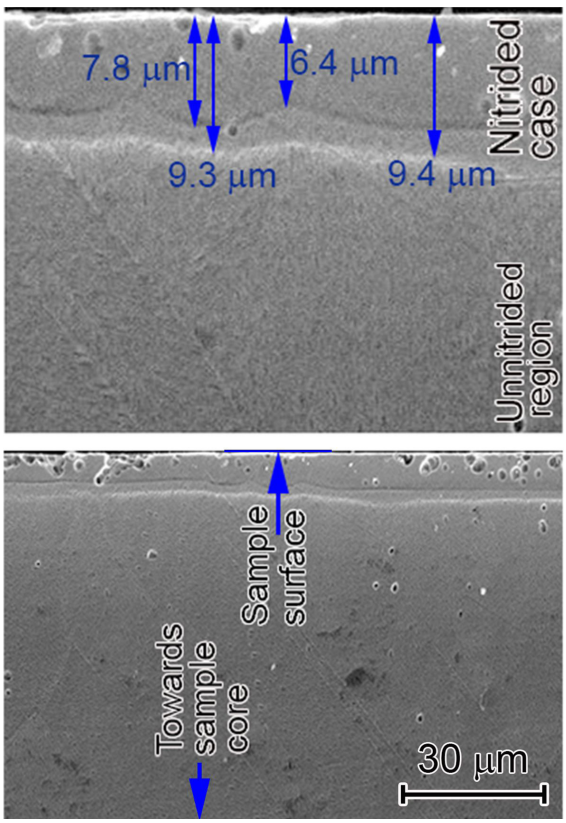

Figure 2. Transversal section micrograph of a nitrided sample. SEM. Electrolytic etching, 10g oxalic acid + 100 ml distilled water. Secondary electrons. 15 kV. 20 mm working distance.

On the one hand, with reports in the literature as a basis[2,4], assuming a surface layer of 50 nm for EBSD detection, and comparing it with the thickness of the nitrided case (9.5 µm), we can conclude that the EBSD patterns in this experiment are superficial. On the other hand, in this contribution, the electron beam size was around 10 nm, while EBSD scanning step was around 3 µm and austenitic grain size was around 30 µm. In conclusion, with regard to the typical length of austenitic microstructure and nitrided case depth in this experiment, it can be straightforwardly assumed that the EBSD interaction volume is very small.

An almost flat interface between the nitrided and non-nitrided regions was observed. Nitriding treatment induced a meaningful hardening of the treated material. Hardness was increased from 3.0±0.5 GPa to 14.4±1.6 GPa, as a consequence of nitriding. The high error of on-top hardness in as-nitrided virgin surfaces was associated with surface roughening, which was induced by the nitriding process itself. A mild variation of nominal hardness between the as-nitrided virgin surface and the polished surface was observed. Hardness decreased from 14.4±1.6 GPa to 13.0±0.6 GPa, as a consequence of surface polishing. The mild reduction in hardness after mechanical polishing was attributed to the fact that only 15% of the nitrided case was removed.

Hardness reported elsewhere for the expanded austenite phase, obtained by diverse plasma nitriding processes of conventional ASSs, typically ranges between 7 and 16 GPa[21,22,31-34].

Figure 3 shows the X-ray scans made on top of (i) as nitrided samples, and (ii) samples with remotion of 1.5 µm of the nitrided case. In Figure 3 an intense shift of the reflections of the austenitic phase for lower Bragg angles because of the nitriding process can be seen. A straightforward correlation between solid solution dissolution of nitrogen in austenite and reflection shifting to lower Bragg angles can be suggested. This is in concordance with the almost absence the nitrogen rich compound phases in the nitride case. After comparing the X-ray scans of the (i) as nitride sample, and the (ii) polished sample, a decrease of the solid solution nitrogen can be pointed out (with regard to the position of the XRD reflections, which are presented at higher Bragg angles for the sample polished).

Figure 3 suggests a tenuous formation of nitrogen rich compound phases. The fraction of this phases is not expressive enough to allow the formation of indexable diffraction reflections. However, qualitatively, it can be suggested a reduction in the intensity of this second phase precipitation in the samples polished with regard to the as-nitrided surface.

Both, the decreasing of solid solution dissolved nitrogen and the less intense precipitation of second phases are suggested as two main factors leading to hardness decrease on the on-top region after some fraction of the nitrided case is removed (hardness decreased from 14.4±1.6 GPa to 13.0±0.6 GPa).

Results shown that the polished surfaces present measurable differences with regard to the virging surface. Those differences can be mainly attributed to a decrease of the overall nitrogen content as the distance to the surface is increased, with is a typical result in plasma nitrided steels.

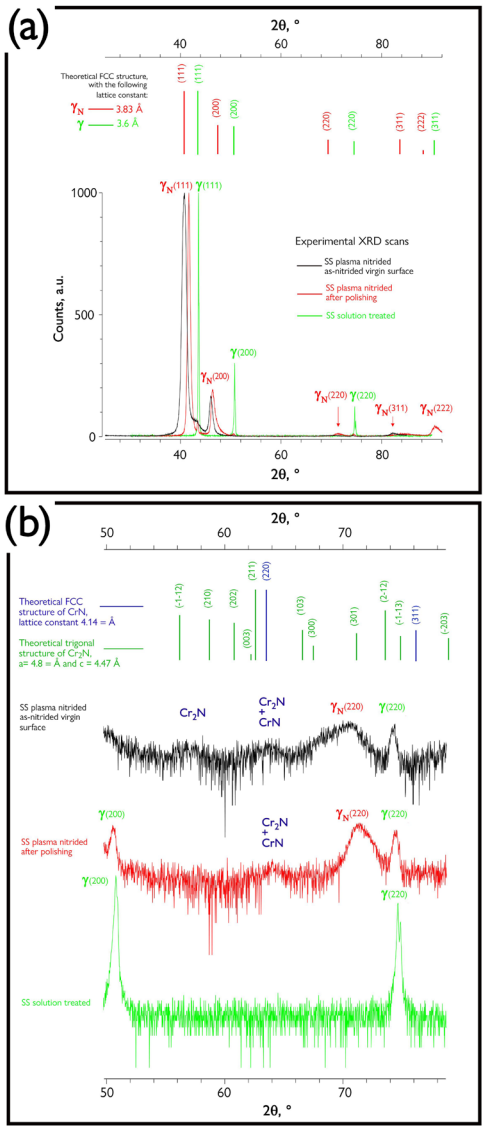

Figure 3. Diffraction patterns on the Bragg-Brentano geometry for the samples (i) solid solution treated, (ii) as plasma nitrided, and (iii) polished. CuK-α radiation. Raw data are presented; i.e., no data-cleaning nor data-fitting procedures were carried out.

3.2. Changes in surface topography as a consequence of mechanical polishing

Figure 4 shows the evolution of the surface appearance, appraised by AFM micrographs, through the stages of grinding and polishing. Figure 5 shows the evolution of the average surface roughness, appraised by the profile roughness parameter Sa, through the stages of mechanical polishing. Sa is an amplitude parameter that is appraised from the arithmetical mean deviation of an appraised profile.

Inset (a) in Figure 4 shows the formation of sharp hills and valleys in the surface of the as-nitrided sample. Figure 5 shows a steep increase in the roughness parameter as a consequence of the nitriding treatment. That surface roughening can be assigned mainly to plastic deformation in the nitrided case[35,36]. Different intensities of plastic deformation toke place at the different austenitic grains (Figure 4), inducing steep changes in the surface topography at the intergranular regions. In particular, triple junctions showed sharper variations in surface roughening. The average surface roughness (Sa) increased from 10 nm to 50 nm as a consequence of the nitriding treatment (Figure 5). Grinding in Al_2O_3 slurries induced Sa roughness decreasing, whereas polishing in colloidal silica almost did not affect the Sa roughness. It should be emphasized that average Sa surface roughness was assessed from AFM scans in a 70 x 70 μm^2 area, given that the results were affected by both intra- and intergranular roughness.

Figure 6 shows the evolution, through the stages of grinding and polishing, of the on-top appearance of selected Berkovich imprints (insets a through d), as well as the profile inside the indentations (insets e through h). Figure 7 shows the diverse profiles acquired from the inside of one representative Berkovich indentation that was imprinted on the sample that was ground in Al_2O_3. From a set of profiles, obtained in different indentations, similar to the one in Figure 7b, we assessed that the resolution in the thickness of the total removed layer was around 100 nm. The main factors affecting the resolution of the residual indentation depths were the anisotropic character of the profiling inside each indentation (Figure 7) and the smoothing of the transition between the inside and outside areas of each indentation, as a consequence of the polishing process (Figure 6). Thus, the thicker the removed layer, the higher the uncertainty in the thickness of such removed layer.

For appraising an eventual losing of parallelism between the polished surface and the as-nitrided virgin surface, the polished depth was computed in each of the four corners of the reference frame. By comparing how much material was removed in each of these corners, it was assessed that the maximum inclination of the polished surface, with regard to the as-nitrided virgin surface, was lower than 0.10°±0.05°.

Figure 8 shows the thickness of the removed layer through the stages of grinding and polishing. The high wear rate during grinding (around 0.10 μm·h^{-1}), with regard to the polishing stages (around 0.0001 μm·h^{-1}), can be noted. Contrasting Figure 4 (surface appearance) and Figure 8 (thickness of the removed layer), it can be stated that the removal of material in the grinding stage is more focused on the regions with high hills; whereas in the polishing stage, the removal of material is more evident inside of individual grains.

3.3. Suitability of the polished surfaces for conducting EBSD characterization of the nitrided layer

Nitrided virgin surfaces were inadequate for obtaining Kikuchi diffraction patterns in the EBSD facility, which was attributed to the intense surface roughening induced by the nitriding process (Figure 4, inset a). Stinville et al.[18] associated surface roughening observed in nitrided samples with plastic deformation triggered by the absorption of nitrogen.

Figure 9 shows selected Kikuchi diffraction patterns, and their concomitant Hough transforms, for an annealed and a nitrided samples.

In EBSD, the Hough transform is used for easy identification of the diffraction bands in the Kikuchi diffraction patterns.

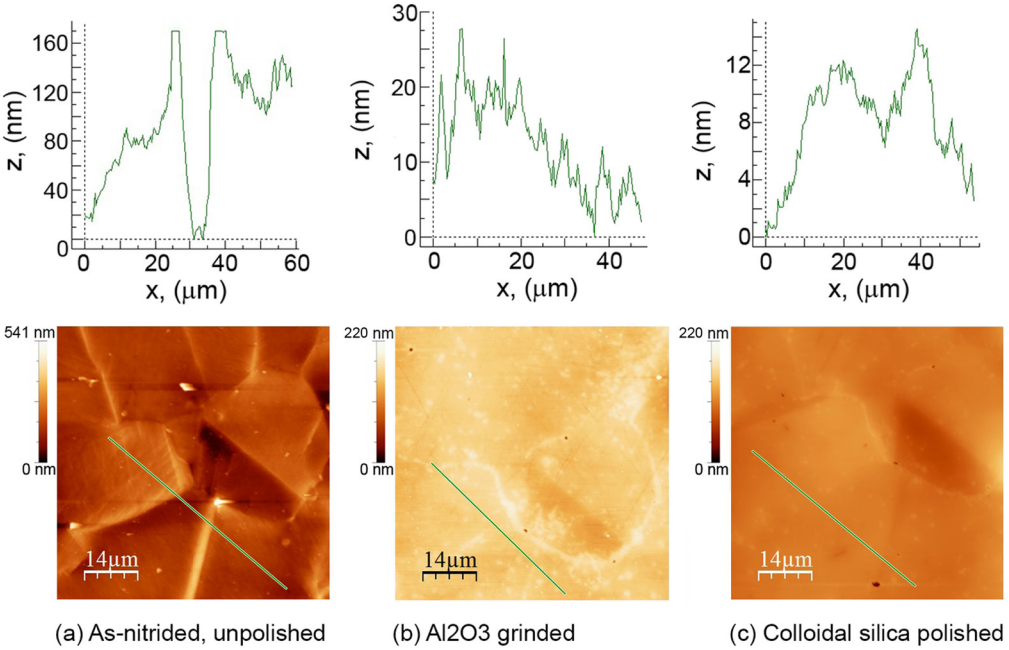

Figure 4. Atomic force micrographs of the appearance of sample surfaces through the stages of grinding and polishing. The reader is advised that the same region was scanned.

The digitalized image of the Kikuchi diffraction pattern is mathematically operated via the Hough transform[1,2], and is obtained as an image in the Hough space, where the original Kikuchi diffraction bands are correlated to circular regions of maximum intensity in the Hough space.

In Figure 9, it can be seen that well-defined Kikuchi diffraction patterns were obtained in the polished samples. Those Kikuchi diffraction patterns lead to Hough transforms with well-defined regions resulting from the diffraction bands (spots in the Hough space). In general, the observed Kikuchi diffraction patterns, and the concomitant Hough transforms, are sharp enough for assessing the local orientation of crystals in the samples analyzed. However, it can be seen in Figure 9 (insets b and e) that the Hough transform of the annealed sample displayed better defined spots of the diffraction bands. We ascribed the lessened resolution observed in the Hough space for the nitrided sample to residual stresses triggered by plastic deformation in the nitrided case. That could be induced by lattice rotations[31] or statistically stored dislocations (SSDs)[37]. Microregions with high density of SSDs are associated to a net zero Burger vector however with incoherent scattering, which lessens the quality of the diffraction patterns[37]. The residual stresses above-referred could not be associated with the grinding and polishing stages (as discussed earlier with Figure 5 as a basis), but we correlated them to the nitriding process itself[23]. According to Tromas et al.[25], thicker removed layers allow for retrieving more reliable EBSD patterns.

The indexing success rate in the annealed samples was 95.6%, whereas it was 88% in the nitrided samples. The increased fraction of unindexed points in the nitrided sample was attributed to the presence of microregions with blurry appearances of the Kikuchi diffraction patterns, which were almost absent in the annealed sample.

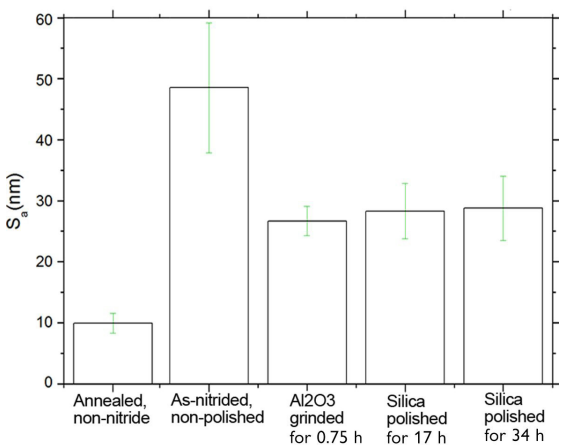

Figure 5. AFM-assessed average surface roughness through the stages of grinding and polishing.

Figure 10 shows the appearance of a selected Kikuchi diffraction pattern, and the concomitant Hough transform, obtained in a microregion of a nitrided sample where the appearance of the diffraction patterns was blurry. We associated those microregions displaying blurry diffraction patterns with the precipitation of nitrogen-rich second phases. However, that second phases were not coarse enough to allow crystallographic characterization by EBSD. Thus, likely presence of statistically stored dislocations cannot be decisively discarded.

Figure 11 shows the histogram of the mean angular deviation (MAD) in EBSD scans of both an annealed and a nitrided sample. MAD is a merit factor that indicates the misfit between the angular distribution of computed

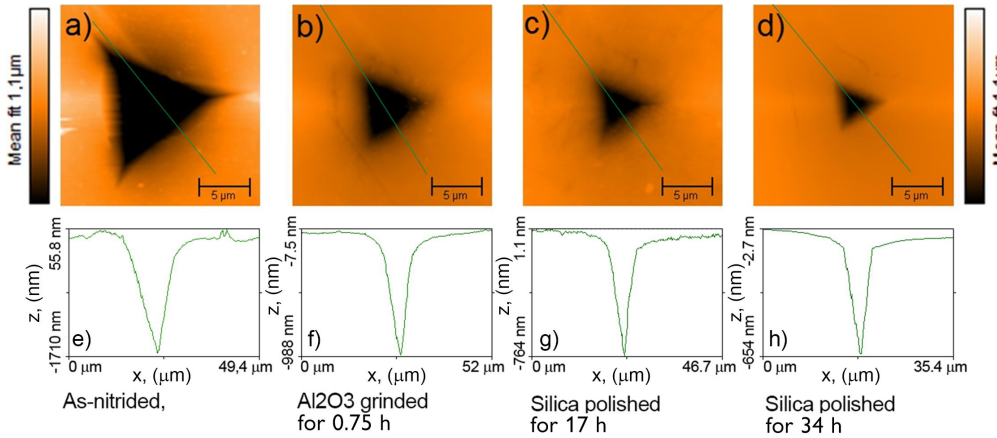

Figure 6. Atomic force micrographs of the appearance, through the stages of grinding and polishing, of the on-top Berkovich indentations (insets a through d), and the profile inside the indentations (insets e through h).

diffraction bands and the experimental bands observed in the Kikuchi diffraction patterns. In general, MAD values lower than 1.0 are desired. In MAD histograms (Figure 11), it can be seen that there is no meaningful degradation of the MAD index in nitrided samples. The relative fraction of indexed patterns with an MAD higher than 1.0 is minimal.

Figure 12 shows the band contrast (BC) map, inverse pole figure (IPF) map, grain boundary character map, and local misorientation map for representative scanned areas in both the annealed and nitrided samples.

Although the BC map in the annealed sample is less dark than in the nitrided sample (Figure 12, insets a and f), no meaningful degradation of the BC index in the nitrided sample can be addressed. BC is a merit index that indicates how well defined the Kikuchi diffraction patterns are. Higher BC indexes are desired.

IPF maps (Figure 12, insets b, c, g, and h) show that EBSD scans provide enough information for adequately assessing the microtexture. Inside each individual grain, several scanned points are indexed, allowing an adequate assessment of the average crystallographic orientation of individual grains.

Local misorientation maps (Figure12) suggest the ability of analyzed scans to provide insight into the variations of lattice orientation at the sub-grain length. The local misorientation approach is especially valuable for assessing the degree of deformation strain in the microstructure[37].

Grain boundary character maps (Figure 12, insets d and i) adequately exhibit the grain boundary character distribution in microstructure, excepting some areas whit impaired ability to characterize parallel grain boundaries nearly located. Similar results can be observed in the Figure 7 of the contribution of Gallo and Dong[35]. This was not associated with the mechanical polishing itself. This was attributed to a combination of the scanning step used in EBSD scans (namely, 3 µm) and the lessened indexing success rate in the sample nitrided. In EBSD characterization, "large" scanning steps are used for assessing the crystallographic orientation of microstructure in lengths that are comparable to the grain size, whereas "small" scanning steps are

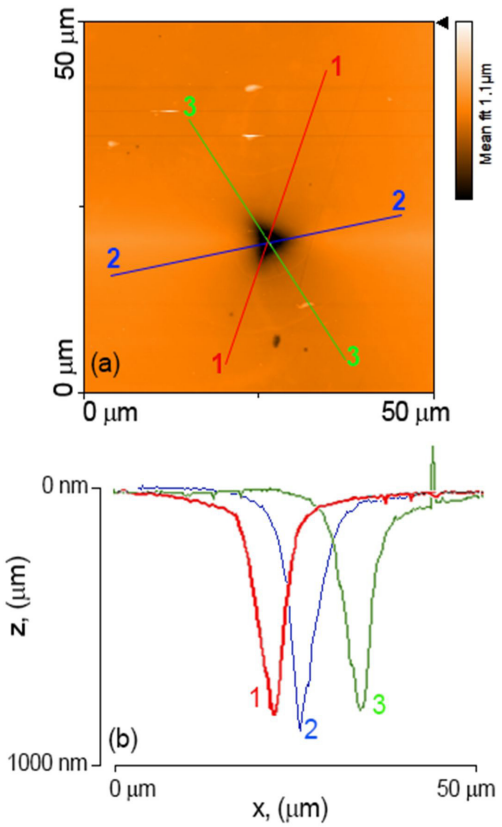

Figure 7. AFM-assessed profiles (b) from the inside of one representative Berkovich indentation (a).

used for assessing the local variations of crystallographic structure at the substructure length. Figure 13 shows a grain boundary character map obtained with an EBSD scan that is carried out with a reduced scanning step (namely, 0.5 µm). Figure 13 also shows that the samples studied allow an EBSD analysis with enough quality for assessing the grain boundary distribution character, provided that small scanning steps are used.

4. Analysis and Discussion

In this contribution, nitrided samples were mechanically polished and the suitability of the polished surfaces for conducting EBSD characterization was appraised. We showed that removed layers as thin as 1.4 µm could be enough for adequate microtexture analysis of the nitrided case, provided that a dual-stage mechanical grinding and polishing procedure was used. Gallo and Dong[35,36] analyzed, via EBSD, the surface of a 316L SS processed by either active-screen plasma nitriding (ASPN)[36] or active screen plasma carburizing[35]. They pointed out that "a fine polishing step with colloidal silica was necessary to obtain good diffraction patterns from the nitrided specimens"[36]. They did not report the parameters used in the post-nitriding polishing stage. We assumed that nitrided or carburized surfaces obtained by them are less rough that the surfaces obtained in this contribution, due to the improved indexability in the Kikuchi diffraction patterns reported by them[35,36]. Consequently, the intense surface roughening observed in this contribution, which greatly hindered sample preparation of post-nitrided specimens, could not be solely addressed to nitrogen absorption. Instead, erosive roughening induced by the energetic sputtering species should be considered also, in samples in this contribution. That sputtering of the nitriding surface by energetic particles most probably is reduced in the ASPN approach reported by Gallo and Dong[35,36].

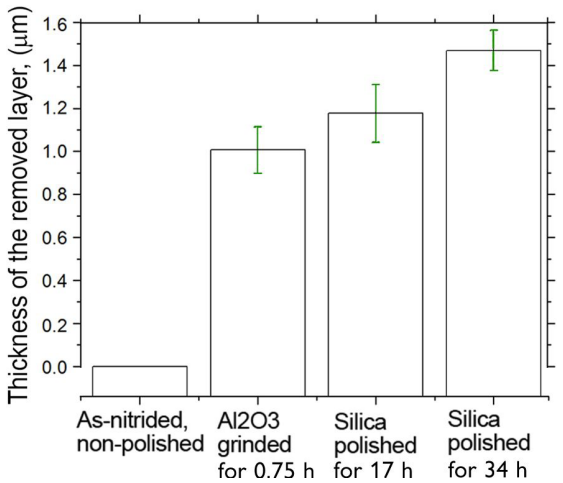

Figure 8. Thickness of the removed layer, through the stages of grinding and polishing.

Asgari et al.[33] prepared, via electro polishing, the surface of an 316L SS pulsed plasma nitrided. They analyzed the as-nitrided surface and the subsurface region, exposed by electro polishing. One can see in Figure 5 in the reference [28], a mild variation of nominal hardness between the as-nitrided virgin surface and the polished surface was observed. Hardness decreased from 14.4±1.6 GPa to 13.0±0.6 GPa, that the indexing success rate is significantly improved in the polished sample vs the virgin as nitrided surface. Different from the results reported for Asgari et al.[33], samples studied in this contribution did not allow obtaining perfectly well-defined Kikuchi diffraction patterns in the as-nitrided surfaces. We addressed this to both the (i) above-referred erosive roughening induced by the energetic sputtering itself and (ii) the electro polishing stage prior to the nitriding process performed by Asgari et al.[33].

Plasma nitrided and plasma carburized surfaces of austenitic SS show impaired Kikuchi diffraction patterns in EBSD analysis[31,33-36,38]. We ascribed this to both surface roughening and residual stresses induced by lattice rotations[18]. Characterization via EBSD of cross-sectioned nitrided structures, in diverse types of steels, shows full indexability of Kikuchi diffraction patterns[19,39,40]. Thus, we can address to the

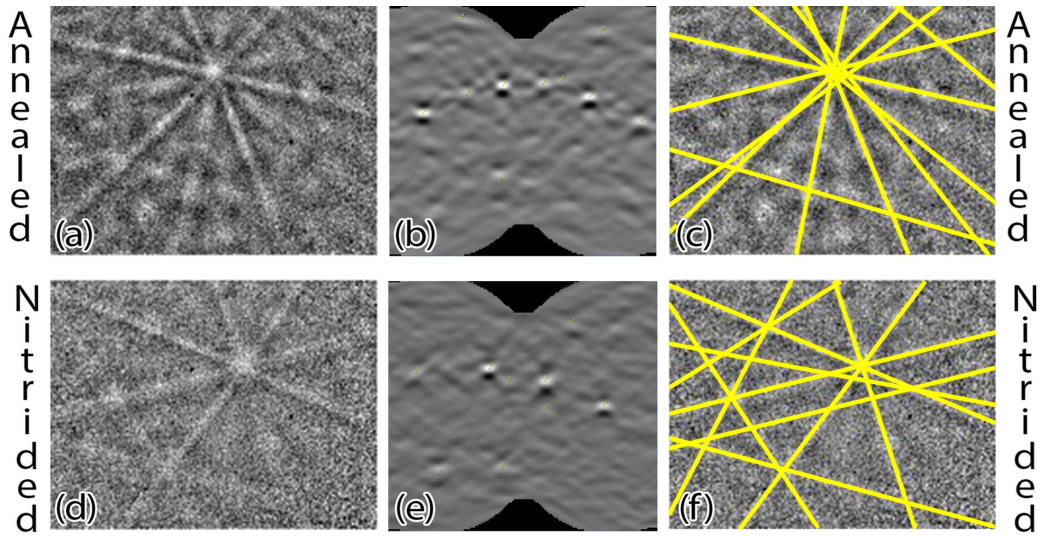

Figure 9. Representative appearance of both Kikuchi diffraction patterns (a and d) and Hough transforms (b and e) for an annealed sample (a to c) and a nitrided sample (c to d). The correlated Kikuchi bands indexed from points detected in the Hough space are also shown (c and f). The diffraction patterns were acquired under the very same conditions used for fast (21 indexed patterns by second) automated pattern processing during the area scanning.

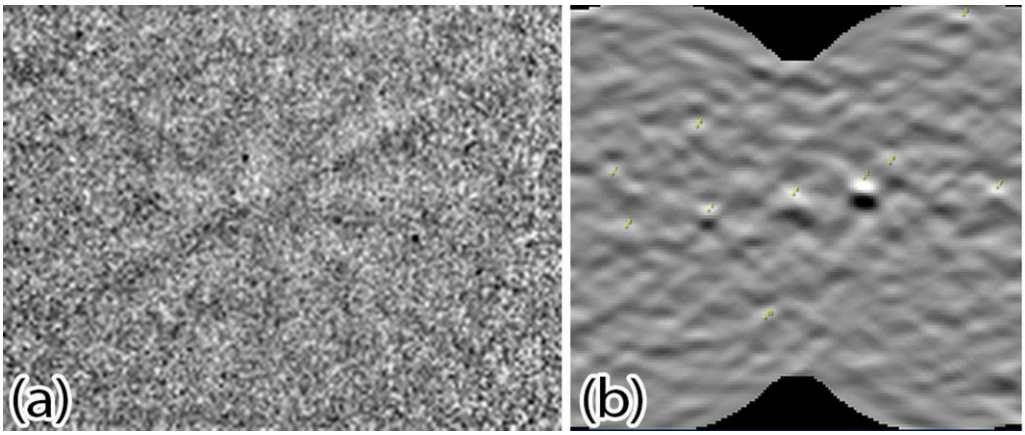

Figure 10. (a) Kikuchi diffraction pattern and (b) Hough transform for a nitrided sample in a microregion where the diffraction patterns were blurry. Degradation in the resolution of those diffraction patterns was ascribed to the precipitation of N-rich second phases.

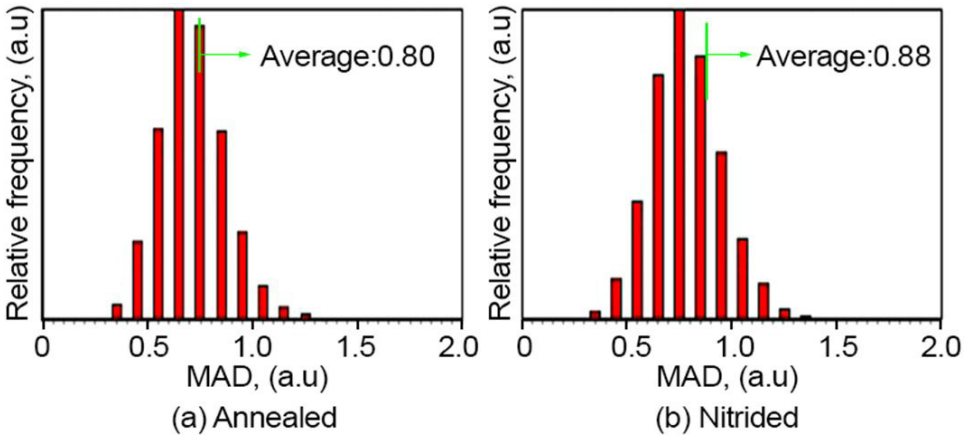

Figure 11. MAD histograms in EBSD scans of annealed (a) and nitrided (b) samples. The mild increase in the average MAD in the nitrided sample should be noted. In general, in EBSD characterization, MAD values lower than 1.0 are aimed at.

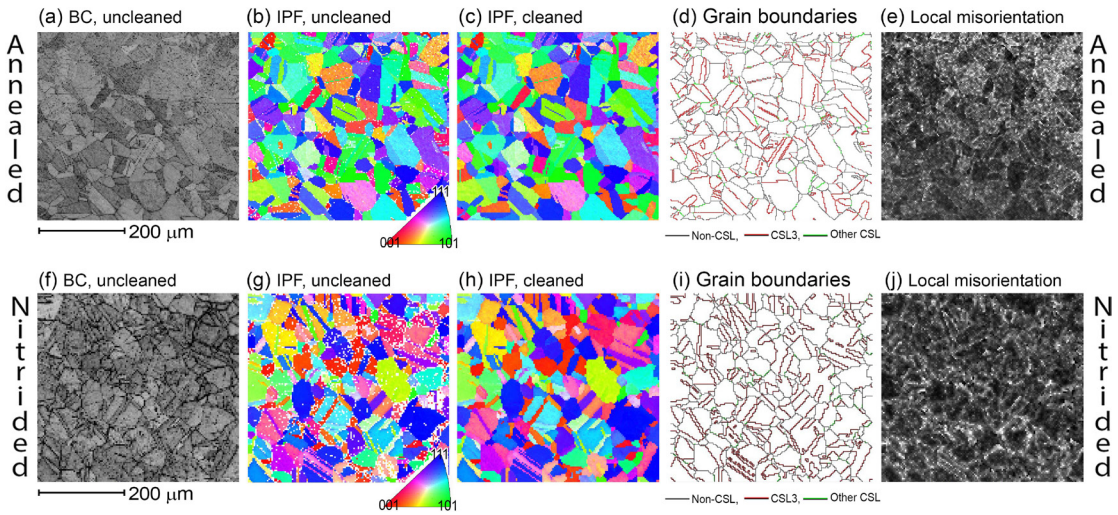

Figure 12. Band contrast (BC) map (a and f), inverse pole figure (IPF) map (b, c, g, h), grain boundary character map (d and i), and local misorientation map (e and j) for representative scanned areas in both the annealed (a to e) and nitrided (f to j) samples. For simplification, a fraction of the actual scanned area is presented. For a comparison, IPF maps of both uncleaned data (b and g) and cleaned data (c and h) are shown.

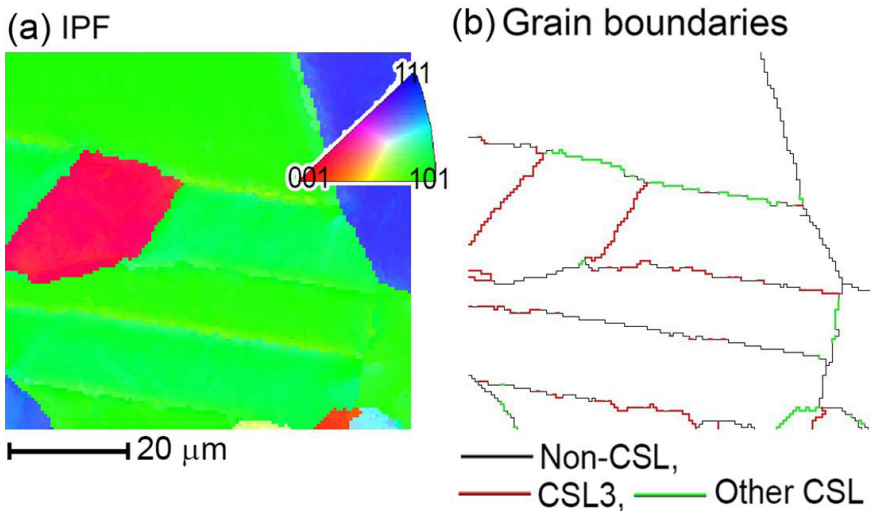

Figure 13. (a) Inverse pole figure (IPF) and (b) grain boundary character map, for a sample nitrided. The scanning step was 0.5 μm. This aimed at characterizing parallel grain boundaries that were closely situated.

deformation stresses only a fraction of the loss in resolution of Kikuchi diffraction patterns, in EBSD characterization of on-top nitrided surfaces.

The results in this contribution showed that the major role of the grinding stage was to accelerate the reduction of the relief between the highest hills and the deepest valleys in the intergranular regions. However, the reasonably high roughness inside individual grains, after grinding, makes Al_20_3 grinding not suitable as the latest polishing stage for posterior EBSD characterization. At our best effort, we did not find previous reports where a post-nitriding grinding stage is carried out in preparing the nitrided surface for EBSD analysis.

In Figure 4, it can be seen that the average roughness of the worn surfaces is mainly controlled by the Al_2O_3 grinding stage, whereas a minor variation of the average roughness is induced by the colloidal silica polishing. However, in Figure 3 (insets b and c), it can be seen that the appearance of the surface inside individual grains is mainly controlled by the colloidal silica polishing: a rather smooth surface inside individual grains is observed in the polished sample (inset c), whereas a roughened and scratched surface inside individual grains can be seen in the ground sample (inset b). It is worth to recall that the polishing rate in colloidal silica was around 0.8 $nm \cdot kh^{-1}$, while in Al_2O_3 it was around 100 $nm \cdot kh^{-1}$.

Post-nitriding mechanical polishing in colloidal silica, without early Al_20_3 grinding, demands for large thickness of the removed layer[25]. We attributed this to the hindered ability of polishing in colloidal silica for attenuation of the relief between the highest hills and the deepest valleys in the intragranular microstructure. However, polishing in colloidal silica is mandatory, due to its ability to produce smooth surfaces inside individual grains[1-3].

The procedure for sample preparation presented in this contribution is time consuming. This involves characterization in the AFM facility, where tiny fiduciary indentations should be located for measuring the depth of the residual impressions. However, this polishing procedure can be associated with (i) high accuracy in the thickness of the removed layer, (ii) low mismatch between microstructure components in the original and the polished surfaces, (iii) high parallelism between the original and the polished surfaces, (iv) and low polishing-induced plastic deformation.

Serial sectioning reported in literature[18,41], based on tracking of the indentation diagonals of fiduciary Vickers imprints, is susceptible to high errors arising from (i) unknowns in the actual relationship between surface diagonals and trough-thickness depth of the indentations, and (ii) either pile-up or sink-in around the imprint borders. Tracking of the diagonal size of Vickers indentations demands a simpler and straightforward analysis. However, the uncertainty in the assessment of the Vickers imprint depth (around 0.1 mm) is excessively high, inhibiting to carry out an exact determination of the inclination of the polished plane. Templier et al.[41] reported 0.1 μm for the uncertainty of the removed layer thickness, for monitoring of the removed layer through the analysis of on-top diagonals of Vickers indentations. They did not report the experimental procedure followed for assessing that uncertainty. In this contribution, via indentation profiling by AFM, we observed that, as the polishing process advances further, the borders of the imprint between the inside and the outsides regions became less defined. Thus, the ratio between the indentation diagonals and the residual depth changes as the polishing procedure advances. This additional error source should be considered in assessing the uncertainty of the removed layer thickness, when it is retrieved from the on-top diagonals of Vickers indentations[41].

The approach of AFM tracking of the removed layer thickness reported in this contribution, based on profiling inside actual indentation imprints, allows an accurate assessment of the thickness of the removed layer. However, this procedure is prone to spurious data if wear debris or abrasive particles are drawn into the hardness imprints. Thus, careful ultrasonic vibratory cleaning before each AFM characterization is mandatory. In addition, tracking of the residual indentation

depth at various hardness imprints is highly recommended, where dirtied imprints should be discarded.

Mechanically polished surfaces are prone to variations in the inclination of the polished surface through the diverse stages of sample preparation. This was kept at a minimum in this contribution, by using sample holders with a homogeneously distributed weight. This mechanical polishing, when associated with AFM tracking of the removed layer thickness, allows an accurate control of the parallelism between the virgin and the polished surfaces. The inclination between the later polished surface and the former as-nitrided virgin surface (0.10°±0.05°) that we have assessed was one order of magnitude lower than the angular uncertainty in the automated high-speed indexation of Kikuchi diffraction patterns, which is roughly 1°[1]. This enables accurate determination of lattice rotations in micrometric lengths, induced by nitriding.

5. Summary

We reported on a dual-stage grinding and polishing method that was optimized for preparing the nitrided region of an ASS for crystallographic characterization of the microstructure via EBSD experiments. This method warrants high sensibility in the control of the total removed layer and leads a high degree of parallelism between the later polished surface and the former as-nitrided surface. Regarding the suitability of the polished surfaces for conducting EBSD characterization, the following conclusions can be stated:

1. Polished surfaces, obtained after removing layers as thin as 1.4 μm (15% of the total nitrided case), were adequate for microtexture analysis of the nitrided case.
2. For removed layers 1.4 μm thick, Hough space associated with the Kikuchi diffraction patterns showed a somewhat lack of resolution in the nitrided case, with regard to the non-nitrided material. This was addressed to nitrided-induced work-hardening effects.
3. A decrease in the indexing success rate from 95.6% to 88% was induced by the presence of second phases in the nitrided samples.
4. The fraction of unindexed diffraction patterns in the nitrided samples (around 12%) did not hamper the adequate characterization of the microtexture, which was sufficiently assessed because several indexed points were obtained for each individual grain.
5. The major effect of grinding in Al_2O_3 slurries was the preferential wear of the intragranular regions in the roughened surfaces, which allowed one to restrain the thickness of the total removed layer.
6. The profiling inside fiducial Berkovich imprints allowed one to assess both the thickness of the removed layer with a resolution of 100 nm, and the valuation of the maximal angular deviation from parallelism between the polished and the original surfaces, which was around 0.10°±0.05°.

6. Acknowledgements

The authors acknowledge the financial and structural support provided by the Santa Catarina State University (UDESC), and the Thin Films, Surface Science, and Plasma Lab Facility (LPFS), Brazil.

7. References

1. Wilkinson AJ, Britton TB. Strains, planes, and EBSD in materials science. Mater Today. 2012;15:366-76.
2. Stojakovic D. Electron backscatter diffraction in materials characterization. Process Appl Ceram. 2012;6:1-13.
3. Schwarzer RA, Sukka J. Electron back scattered diffraction: current state, prospects and comparison with x-ray diffraction texture measurement. Banaras Metallurgist. 2013;18:1-11.
4. Randle V. Applications of electron backscatter diffraction to materials science: status in 2009. J Mater Sci. 2009;44:4211-8.
5. Vincentis NS, Roatta A, Bolmaro RE, Signorelli JW. EBSD analysis of orientation gradients developed near grain boundaries. Mater Res. 2019;22:e20180412.
6. Souza SH, Padilha AF, Kliauga AM. Softening behavior during annealing of overaged and cold-rolled aluminum alloy 7075. Mater Res. 2019;22:e20180666.
7. Bulutsuz AG, Yurci ME, Durakbaşa N. Optimization process parameters of equal angular channel pressing according to the measurement results of microstructural homogeneity. Mater Res. 2018;21:e20180270.
8. Vander Voort GF, Pinard P. Specimen preparation of metals and alloys for EBSD. Microsc Microanal. 2011;17:416-7.
9. Britton FJ, Jiang J, Guo Y, Vilalta-Clemente A, Wallis D, Hansen LN, et al. Tutorial: crystal orientations and EBSD - or which way is up? Mater Charact. 2016;117:113-26.
10. Humphreys FJ. Grain and subgrain characterization by electron backscatter diffraction. J Mater Sci. 2001;36:3833-54.
11. Fan HY, Liu SF, Guo Y, Deng C, Liu Q. Quantifying the effects of surface quality on texture measurements of Tantalum. Appl Surf Sci. 2015;339:15-21.
12. Wright SI, Nowell MM. EBSD image quality mapping. Microsc Microanal. 2006;12:72-84.
13. Foltz J, Hugo R. Recent advances in EBSD deformation analysis. Adv Mater Process. 2016;174:21-4.
14. Kamaya M. Assessment of local deformation using EBSD: quantification of local damage at grain boundaries. Mater Charact. 2012;66:56-67.
15. Rodríguez MG, Martínez EE, Torres G, Escalera MD. Metallographic preparation of Zn-21Al-2Cu alloy for analysis by Electron Backscatter Diffraction (EBSD). Microsc Microanal. 2014;20:1276-83.
16. Nowell MM, Wright SI, True B. EBSD sample preparation: techniques, tips, and tricks. Micros Today. 2005;13:44-9.
17. Zhao Y, Yu B, Dong L, Du H, Xiao J. Low-pressure arc plasma-assisted nitriding of AISI 304 stainless steel. Surf Coat Tech. 2012;210:90-6.
18. Stinville JC, Villechaise P, Templier C, Rivière JP, Drouet M. Lattice rotation induced by plasma nitriding in a 316L polycrystalline stainless steel. Acta Mater. 2010;58:2815-21.
19. Proust G, Retraint D, Chemkhi M, Roos A, Demangel C. Electron backscatter diffraction and transmission Kikuchi diffraction analysis of an austenitic stainless steel subjected to surface mechanical attrition treatment and plasma nitriding. Microsc Microanal. 2015;21:919-26.
20. Zhang ZL, Bell T. Structure and corrosion resistance of plasma nitrided stainless steel. Surf Eng. 1985;1:131-6.
21. Vianna AM, Brunetti C, Mafra M, Reis RF, Villanova RL, Bernardelli EA. Plasma nitriding of ISO 5832-1 stainless steel at 425 ºC with Intermittent nitrogen flow. Mater Res. 2020;23:e20200249.
22. Campos M, Souza S, Davim JP, Souza SD, Olzon-Dionysio M. Influence of the gas pressure of plasma nitriding on the structural, mechanical and tribological surface properties of AISI 316L. Mater Res. 2019;22:e20190302.

23. Manova D, Lutz J, Gerlach JW, Neumann H, Mändl H. Relation between lattice expansion and nitrogen content in expanded phase in austenitic stainless steel and CoCr alloys. Surf Coat Tech. 2011;205:S290-3.
24. Sun Y, Li X, Bell T. X-ray diffraction characterization of low temperature plasma nitride austenitic stainless steels. J Mater Sci. 1999;34:4793-802.
25. Tromas C, Stinville JC, Templier C, Villechaise P. Hardness and elastic modulus gradients in plasma-nitrided 316L polycrystalline stainless steel investigated by nanoindentation. Acta Mater. 2012;60:1965-73.
26. Sharma H, Bohemen SMC, Petrov RH, Sietsma J. Three-dimensional analysis of microstructures in titanium. Acta Mater. 2010;58:2399-407.
27. Šedivý O, Jäger A. On correction of translational misalignments between section planes in 3D EBSD. J Microsc. 2017;266:186-99.
28. Zankel A, Wagner J, Poelt P. Serial sectioning methods for 3D investigations in materials science. Micron. 2014;62:66-78.
29. Chen YJ, Hjelen J, Roven HJ. Application of EBSD technique to ultrafine grained and nanostructured materials processed by severe plastic deformation: sample preparation, parameters optimization and analysis. Trans Nonferrous Met Soc China. 2012;22:1801-9.
30. Wirth R. Focused Ion Beam (FIB) combined with SEM and TEM: advanced analytical tools for studies of chemical composition, microstructure and crystal structure in geomaterials on a nanometre scale. Chem Geol. 2009;261:217-29.
31. Li Y, Wang Z, Wang L. Surface properties of nitrided layer on AISI 316L austenitic stainless steel produced by high temperature plasma nitriding in short time. Appl Surf Sci. 2014;298:243-50.
32. Samanta A, Chakraborty H, Bhattacharya M, Ghosh J, Sreemany M, Bysakh S, et al. Nanotribological response of a plasma nitrided bio-steel. J Mech Behav Biomed Mater. 2017;65:584-99.
33. Asgari M, Barnoush A, Johnsen R, Hoel R. Microstructural characterization of pulsed plasma nitrided 316L stainless steel. Mater Sci Eng A. 2011;529:425-34.
34. Singh V, Marchev K, Cooper CV, Meletis EI. Intensified plasma-assisted nitriding of AISI 316L stainless steel. Surf Coat Tech. 2002;160:249-58.
35. Gallo SC, Dong H. EBSD and AFM observations of the microstructural changes induced by low temperature plasma carburising on AISI 316. Appl Surf Sci. 2011;258:608-13.
36. Gallo SC, Dong H. New insights into the mechanism of low-temperature active-screen plasma nitriding of austenitic stainless steel. Scr Mater. 2012;67:89-91.
37. Wright SI, Nowell MM, Field DP. A review of strain analysis using electron backscatter diffraction. Microsc Microanal. 2011;17:316-29.
38. Miyamoto G, Yonemoto A, Tanaka Y, Furuhara T, Maki T. Microstructure in a plasma-nitrided Fe–18 mass% Cr alloy. Acta Mater. 2006;54:4771-9.
39. Schuster J, Bruder E, Müller C. Plasma nitriding of steels with severely plastic deformed surfaces. J Mater Sci. 2012;47:7908-13.
40. Asgari M, Barnoush A, Johnsen R, Hoel R. Small-scale structural and mechanical characterization of the nitrided layer in martensitic steel. Tribol Int. 2013;61:109-15.
41. Templier C, Stinville JC, Renault PO, Abrasonis G, Villechaise P, Rivière JP, et al. Nitrogen interstitial induced texture depth gradient in stainless steel. Scr Mater. 2010;63:496-9.